PULSE WIDTH MODULATION CONTROL OF THREE-PHASE AC-to-DC CONVERTER FEEDING DC MOTOR DRIVE SYSTEMS

التحكم في أنظمة الجر ذات محركات التيار المستمر باستخدام المبدلات ثلاثية الطور العاملة على مبدأ تعديل عرض النبضة

SADEQ A. HAMED

DEPARTMENT OF ELECTRICAL ENGINEERING
FACULTY OF ENGINEERING AND TECHNOLOGY
THE UNIVERSITY OF JORDAN
AMMAN-JORDAN

الخلاصة

يمكن استخدام المبدلات العاملة على مبدأ تعديل عرض النبضة للتحكم في أنظمة الجر ذات محركات التيار المستمر بشكل فعال واقتصادي. تقدم هذه الورقة نموذجا رياضيا لنظام جر ثلاثي الطور يستخدم مبدأ التعديل المتماثل لعرض النبضة. وقد تم تطوير وعرض هذا النموذج بحيث يمكن تطبيقه مهما كان تردد القطع أو التعديل (وبالتالي عدد النبضات لكل دورة تماثل في المخرج). كما تم إثبات صحة النموذج الرياضي عمليا. وتبحث الورقة في تأثير كل من تردد القطع والثابت الزمني للمتحرض على الأداء العام للنظام وخصوصا تيار المتحرض للمحرك. كما تم عرض خصائص الأداء العامة للنظام ومن أهمها خصائص العزم- السرعة، إضافة الى تغيرات معامل التموج لتيار المتحرض ومعامل الإستطاعة للدخل مع تغيرات سرعة المحرك عند قيم محددة لعنصر التحكم وهو معامل التعديل γ.

ABSTRACT

Self-commutated AC-to-DC converters with pulse width modulation (PWM) control can economically and efficiently be employed in DC drive systems of small and medium power ratings. In this paper, a mathematical model for a three-phase AC-to-DC converter feeding DC drive system with uniform pulse width modulation (UPWM) is developed. The model is presented in a generalized form such that it is applicable irrespective of the chopping (or modulating) frequency (and hence the number of pulses per output period of symmetry). The developed model is experimentally verified. The effects of the chopping-to-supply frequency ratio (a control parameter) and the inductance-to-resistance ratio of the motor armature (a design parameter) on the armature current are investigated. The major performance characteristics of the system are also evaluated and presented.

1 INTRODUCTION

DC drive systems of medium and large horsepower applications are conventionally fed from three-phase phase-controlled thyristor converters. The main disadvantages that are usually associated with such converters are significant load ripple factor, poor input power factor and generation of considerable lower-order harmonics in both load and line circuits. Several forced-commutated thyristor converters using different strategies of pulse width modulation (PWM) control have been developed and proved to offer better performance characteristics. But the switching limitations, the design complexity and the cost of such systems prevent this control strategy from being widely applied. However, the implementation of self-commutated converters employing controlled-on and off power switches, such as power transistors, GTOs and IGBTs, allows for this control strategy to be applied economically and efficiently.

Unlike phase-controlled systems, PWM controlled DC drive systems are not popular in literature. The PWM topology that was developed by Kotaoka et al. [1], has emerged as the most popular and satisfactory form of PWM control strategy. Quasi-sinusoidal pulse width modulated DC drive system has been reported in [2]. State equations of (27) different modes of operation, originated due to the forced commutation circuitry, were arranged and numerically solved. Due to the proposed switching pattern, the load and line currents contain all even harmonics, including the 2nd and the 4th components. In [3] and [4], different PWM patterns, developed to reduce the lower order harmonics of the line current, were investigated. The results, based on a simplified analysis of passive R-L load and presented in a normalized form relative to the DC link current which was assumed to have an ideal flat-topped shape, show that the 5-pulse and 7-pulse schemes provide the best possible performance characteristics. Modelling, implementation, and performance evaluation of single-phase DC drive systems with uniform and sinusoidal PWM control were reported in [5-7].

This paper presents a three-phase DC drive system with uniform PWM. A steady-state mathematical model of the system is developed and presented in a generalized form that is applicable irrespective of the chopping frequency (and hence the number of pulses per output period of symmetry). A testing model is implemented to validate the developed model and its solution. The general performance characteristics of the system with a separately-excited DC motor are evaluated and investigated.

2 PRINCIPLE OF OPERATION

Figure (1) shows the circuit configuration of the system under consideration. The power circuit comprises two stages. In the first stage, uncontrolled three-phase bridge rectifier is employed to unify the direction of the load current. In the second stage a power transistor switch, operating in the chopping mode, is used to vary the amplitude of the output average voltage, using uniform pulse width modulation (UPWM) control strategy. Details of the drive circuitry of the power transistor are shown in figure (1).

The principle of (UPWM) control is demonstrated in figure (2-a). A carrier triangular wave $v_c(x)$, having a fixed maximum amplitude V_c, is generated at the required chopping (or modulating) frequency using phase-locked loop (PLL). The carrier wave is compared with a DC level V_m of variable amplitude ($0 \le V_m \le V_c$). The output of the comparator forms the drive signal of the modulating transistor. The ratio of V_m to V_c is defined as the modulation index γ (i.e., $\gamma = V_m / V_c$), which is varied in the range ($0 \le \gamma \le 1$).

Due to the nature of the rectification stage, the output voltage and current waveforms are repetitive at a frequency f_o equals six times the supply frequency f_s (i.e., $f_o = 6 f_s$), with an output period of symmetry, To, equals to $\pi/3$.

The number of pulses in each input period of symmetry (*i.e.*, 2π) is the same as the chopping-to-supply

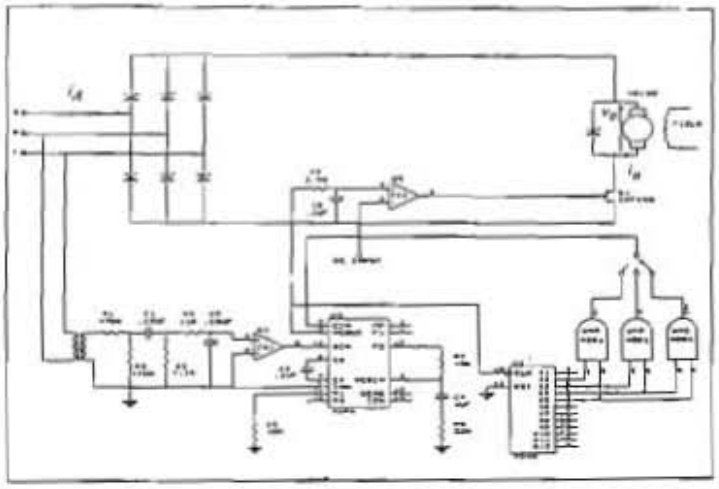

Figure (1): Power-control configuration of the drive system.

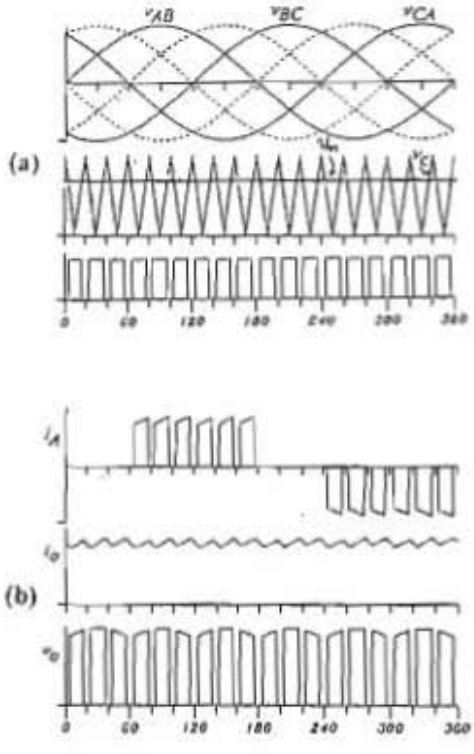

Figure (2): Principle of PWM control and typical waveforms.

(a) Control Signals. (b) Typical waveforms.

frequency ratio M (i.e., $M=f_c/f_s$). M should be a positive integer for purposes of waveform symmetry. This implies that each output period of symmetry comprises a number of pulses N, where N is an integer given by $N = M/6 = f_c/f_n$. For N to be an integer in a *50 Hz AC* system, f_c should be a multiple of *300* (i.e., *300, 600, 900, ...etc.*). Since the *PLL*, employed to generate the required frequency, normally yields 2^k multiples of the supply frequency (i.e., *100, 200, 400, 800 Hz, ... etc.*), the drive unit is accommodated with a logic circuitry to obtain the required value of f_c.

Typical waveforms of the supply current, load current and voltage of the system under consideration are shown in Figure (2-b), where f_c=*900 Hz* (i.e., M=*18* and N=*3* pulses per output period of symmetry).

3 GENERALIZED MATHEMATICAL MODEL

A generalized mathematical model of the system under consideration is developed and presented in the following subsections.

3-1 Switching Boundaries

Over the first period of output symmetry (i.e., $0 \le x < \pi/3$), the nth chopping cycle lies in the range $(n-1)T \le x < nT$, where $n = 1, 2, 3, \ldots, N$ and T is the period of the chopping cycle, given by:

$$T = \frac{2\pi}{M} = \frac{\pi}{3N} = \frac{2\pi}{f_c / f_s} \qquad (1)$$

The conduction of the modulating transistor over the nth chopping cycle lies in the range $\alpha(n) \le x \le \beta(n)$, where $\alpha(n)$ and $\beta(n)$ are respectively the switching-on and off angles of the power transistor over the nth chopping period. These are the intersection points of the modulating wave with the negative and the positive-slope of the carrier wave over the nth chopping period, respectively.

The carrier triangular signal has a generalized analytical expression of the form:

$$v_c(x) = \pm V_c \{(M/\pi)x - 2n + 1\} \qquad (2)$$

The negative and positive signs of *Eqn.(2)* above belong to the negative and positive slopes of the carrier wave, respectively. For uniform *PWM*, the modulating wave is a time-independent *DC* signal given by:

$$v_m(x) = V_m \qquad (3)$$

Equating *Eqns.(2)* and *(3)* and rearranging, the switching instants and, hence, the boundary limits of the nth conduction interval $\alpha(n)$ and $\beta(n)$ are found to be:

$$\alpha(n) = \frac{\pi}{M}(2n - \gamma - 1) \qquad (4)$$

$$\beta(n) = \frac{\pi}{M}(2n + \gamma - 1) \qquad (5)$$

The triangular wave should be synchronized with any of the line voltages in order to obtain the required symmetry of the output waveforms. For this purpose, and since it has the highest positive polarity over the period ($0 \le x \le \pi/3$), the line voltage $Vp\ Sin(\omega t + \pi/3)$ is taken as a reference. For generalization

purposes, the expression $Vp\ Sin(\omega t-\lambda\pi/3)$, with $\lambda=1$ to start with, is taken as a reference. λ is to be incremented by (1) every $\pi/3$ up to $\lambda=7$ if one complete period of the input is to be covered.

The required value of the line voltage is determined by the rated terminal voltage of the motor V_r such that when $\gamma=1$, the average load terminal voltage should equal the rated terminal voltage of the motor. Hence Vp is determined by:

$$V_p = \frac{\pi}{3} V_r \qquad (6)$$

3-2 Conduction Patterns

Depending upon the state of the switching transistor, there are two possible patterns of conduction over each output period of symmetry. The first, *pattern (I)*, corresponds to the on-state periods of the modulating transistor, where the rectified supply voltage appears across the terminals of the armature circuit, forcing a current to flow from the supply into this circuit. This is referred to as the "*pattern of forced current transition*". Applying *Kirchhoff's* voltage law *KVL*, yields:

$$E + R.i_1 + L.di_1/dt = V_p\ Sin(x - \lambda\pi/3) \qquad (7)$$

The second, *pattern (II)*, corresponds to the off-state periods of the modulating transistor, where the load circuit is isolated from the supply and the armature is short-circuited through the freewheeling diode, implying that the load terminal voltage is zero. The armature current will then decay through the freewheeling diode in what is referred to as the "*pattern of current decaying*". Applying *KVL* yields:

$$E + R.i_2 + L.di_2/dt = 0 \qquad (8)$$

General solutions of *Eqns.(7)* and *(8)* for the nth chopping cycle are respectively given by:

$$i_1(n) = I_p\ Sin(x - \lambda\pi/3 - \phi) - I_E + A_1(n)\ e^{\rho x} \qquad (9)$$

$$i_2(n) = - I_E + A_2(n)\ e^{\rho x} \qquad (10)$$

where $A_1(n)$ and $A_2(n)$ are the integration constants. Applying the initial conditions where at $x = \alpha(n)$, $i_1(n) = I_1(n)$ and at $x = \beta(n)$, $i_2(n) = I_2(n)$, substituting in *Eqns.(9)* and *(10)* respectively and rearranging yields:

$$A_1(n) = \{I_1(n) + I_E - I_p\ Sin[\alpha(n) - \lambda\pi/3 - \phi]\}\ e^{-\rho\alpha(n)} \qquad (11)$$

$$A_2(n) = \{I_2(n) + I_E\}\ e^{-\rho\beta(n)} \qquad (12)$$

$I_1(n)$ and $I_2(n)$ are, respectively, the initial currents of the on-state and off-state periods of the nth chopping cycle.

3-3 Solution Procedure

For given modulation index γ and motor speed, it is required to determine the corresponding boundary parameters $I_1(n)$ and $I_2(n)$. This can be accomplished by applying the final conditions, where $i_1(n) = I_2(n)$ at $x = \beta(n)$ and $i_2(n) = I_1(n+1)$ at $x = \alpha(n+1)$. Substituting in *Eqns.(9)* and *(10)* respectively and rearranging yields:

$$I_2(n) = I_p\, Sin[\beta(n)-\lambda\pi/3 -\phi] - I_E + A_1(n)\, e^{\rho\beta(n)} \qquad (13)$$

$$I_1(n+1) = - I_E + A_2(n)\, e^{\rho\alpha(n+1)} \qquad (14)$$

Under steady-state operation, $I_1(1)$ and $I_1(N+1)$ should essentially be equal. For a given value of γ, $I_1(1)$ has to be given an initial value to start an iterative process, developed to evaluate the corresponding boundary parameters $I_2(n)$ and $I_1(n+1)$, from $n=1$ up to $n=N$. The computed value of $I_1(N+1)$ is then used to update $I_1(1)$ for the next iteration step. The above procedure is repeated until the condition for steady state solution {*i.e.*, $I_1(1)=I_1(N+1)$} is achieved, within a certain permissible error.

If the computed values of $I_1(n)$ and $I_2(n)$ are found positive, the load current comprises patterns *(I)* and *(II)* in a repetitive sequence, and the system is said to operate in the *continuous mode* of operation. If any of these currents is found negative, a situation that is only theoretical, then due to the practical limitation of the switching devices, the load current comprises, besides to patterns *(I)* and *(II)*, zero-current gap(s). In such a condition, which usually occurs under light loading conditions, the modulation process is not maintained regular over the complete period of output symmetry, and the motor armature current is discontinuous. This is referred to as the *discontinuous mode* of operation. Over the imposed zero-current gap(s), the armature circuit is open-circuited, and the motor coasts. Over the zero-current gap(s), the back EMF E, a speed-dependent parameter, appears across the motor terminals, forming part(s) of the terminal voltage.

For the discontinuous mode of operation, a similar procedure to that of the continuous mode is followed to evaluate the boundary parameters. The only exception is that it is required here to check, for any value of n, the computed values of $I_1(n)$ and $I_2(n)$. If both are positive, the solution procedure will normally proceed as for the continuous mode of operation. If not, a decision has to be taken as follows:

- If $I_2(n)$ is found negative, then $I_2(n) = I_1(n+1) = 0$.
- If $I_2(n)$ is found positive, then $I_1(n+1)$ is to be calculated from *Eqn (14)*. If it is found negative, it has to be reset zero.

Current expressions (9) and (10) are also applicable for this mode of operation, but with the constraints that if the computed load current for any value of x is found negative, it should be reset zero to match the practical limitation of the switching devices.

The modulation index at which the system moves from one mode of operation to the other (continuous to discontinuous or vice versa), is known as the critical modulation index γ_{cr}.

4 EXPERIMENTAL VERIFICATION

The system of figure (1) is practically implemented and employed to verify the developed mathematical model and its solution. The parameters of the *DC* motor involved in the testing set are given in *Appendix*.

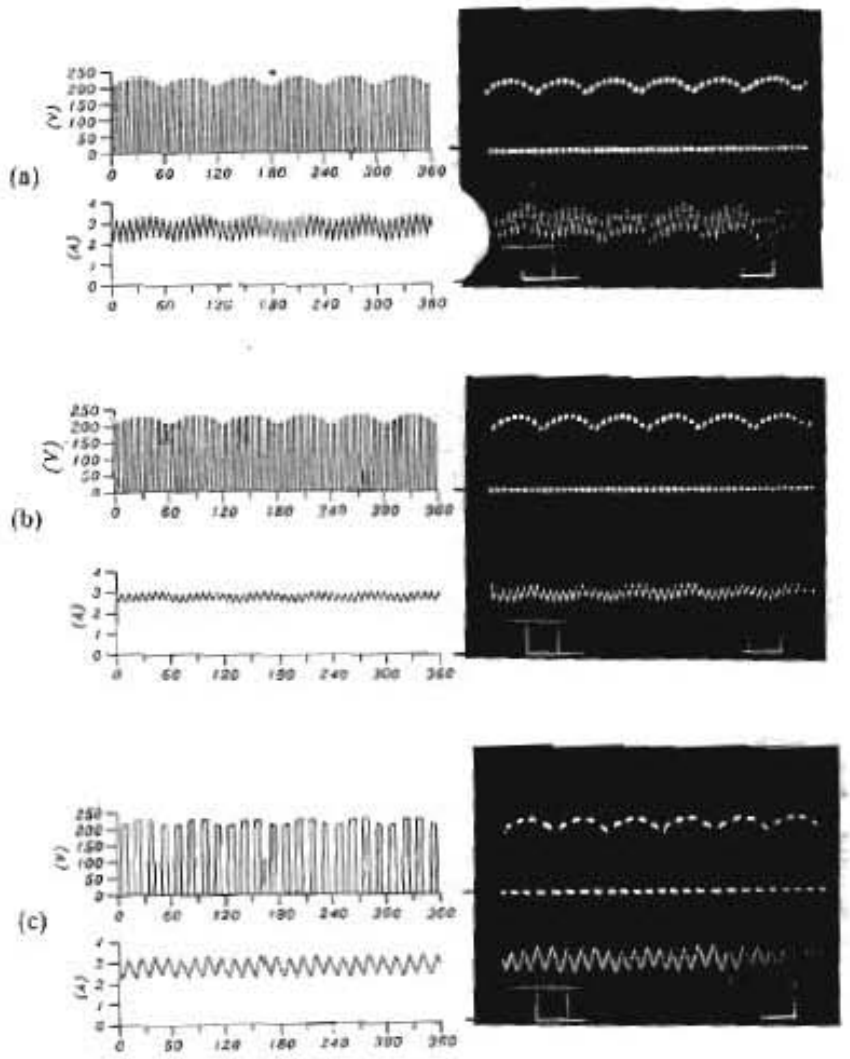

Figure (3): Practical verification of the developed model and solution.

Comparison between experimental and computed load voltage and current waveforms is shown, to scale, in figure (3), where three examples of comparison are provided for the same loading conditions (*1000 RPM* and *1.85 N.m*). Figure (3-a) corresponds to a *chopping frequency* of *2400 Hz* (*8* pulses per output period of symmetry) and original armature *inductance-to-resistance* ratio, figure (3-b) corresponds to the same *chopping frequency* but with an armature *inductance-to-resistance* ratio of *1.5* the original value, and figure (3-c) corresponds to *chopping frequency* of *1200 Hz* (*4* pulses per output period of symmetry) and *1.5* of the original armature *inductance-to-resistance* ratio. It is evident from these examples that good qualitative and quantitative agreement between measured and calculated waveforms is achieved.

5 GENERAL PERFORMANCE EVALUATION

5-1 Critical Operating Limits

For a given speed, critical modulation index γ_{cr} and the corresponding developed torque T_{cr} should be evaluated in order to define the appropriate mode of operation. If the given modulation index (or the given developed torque) is higher than the calculated critical ones, then the system operates in the continuous mode, otherwise, it operates in the discontinuous mode. γ_{cr} is directly related to the motor armature *time-constant* and the converter *chopping frequency*.

The chances for the system to operate in the continuous mode of operation, and hence to improve the performance of the system, can conventionally be increased by the use of DC motors with relatively high armature *time-constant* τ. For the system under consideration, the operation of the converter at a reasonably higher chopping frequencies f_c can also be efficiently used for the same purpose.

Figure (4) shows the variation of the critical developed torque T_{cr} versus the running speed, with the armature time-constant being the parameter. The figure shows that for a given speed, the critical torque is substantially reduced when an external inductance is added in series with the motor armature (i.e., τ becomes higher). This implies improved performance parameters under certain loading conditions.

The influence of the chopping frequency (and hence the number of pulses per output period of symmetry) is also evaluated and presented in figure (5). For a given speed, T_{cr} tends to decrease when f_c is increased.

However, it can be noticed that the influence of both the armature time-constant and the chopping frequency is substantially reduced when any or both of them become sufficiently large.

Figure (6) shows the critical developed torque versus the motor speed for a chopping frequency of *2400 Hz*., and an armature time-constant of *200* % of its original value. The figure shows that over the complete range of speed, the maximum value of the critical torque is less than *0.04 P.U*, implying that the system mainly operates in the continuous mode of operation.

5-2 Load and Line Currents Harmonics

PWM control strategy is expected to yield a reduction in the amplitudes of the lower-order harmonics, and a shift in the orders of the dominant harmonics of the load and line currents. Figure (7) shows typical harmonic spectra of these currents for a chopping frequency of 1200 Hz. Figure (7-a) shows that the harmonics of the orders (6m), where m = 1, 2, 3, ..., are the dominant components of the load current. Of these, the harmonic of the order (M), which is the chopping-to-supply frequency ratio, has the largest amplitude. On the other hand, figure (7-b) shows that the harmonics of the orders (6m±1), where m = 1,

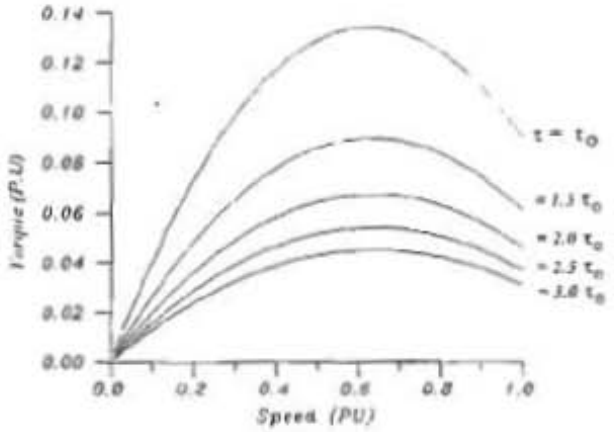

Figure (4): Critical torque versus speed with τ as the parameter.

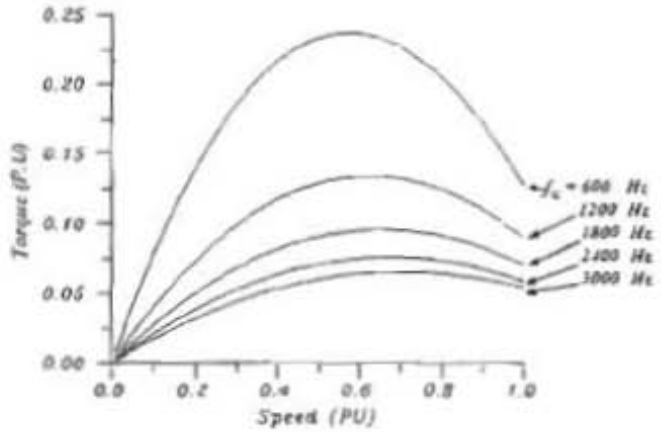

Figure (5): Critical torque versus speed with f_r as the parameter.

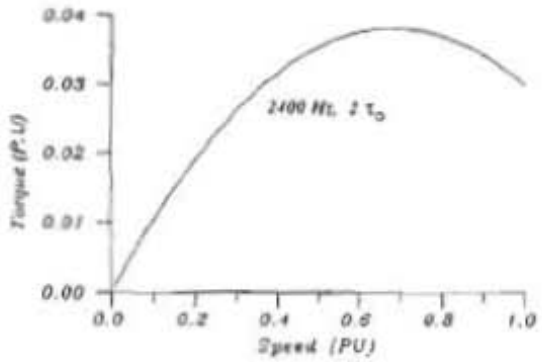

Figure(6): Critical torque versus speed (suggested τ and f_r).

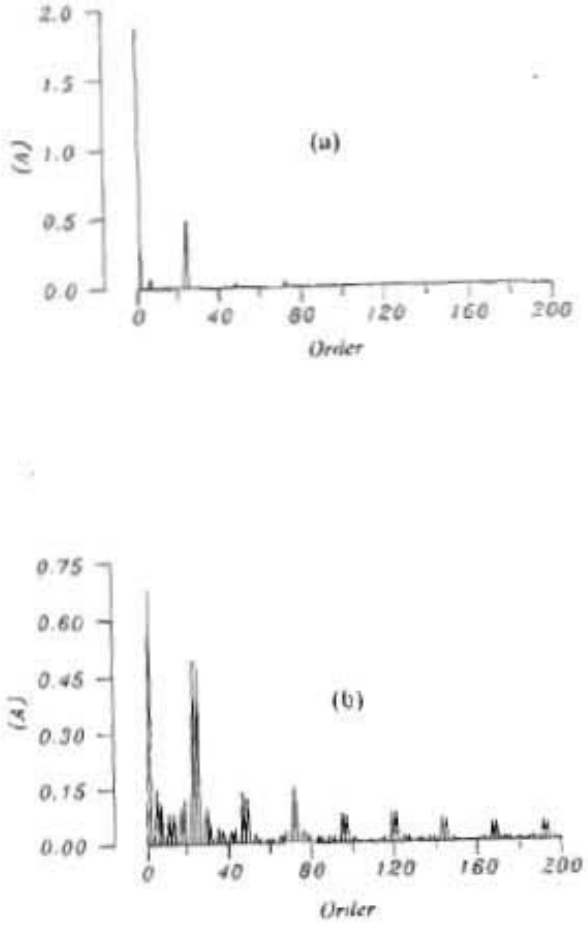

Figure (7): Harmonic spectra of the load and line currents.
(a) Load Current. (b) Line Current.

2, 3, ..., are the dominant components of the line current. Of these, the harmonics of the orders (M±1) have the largest amplitudes. A higher chopping frequency is expected to reduce the amplitudes of the dominant harmonics. It is also expected to increase the orders of these dominant harmonics, implying simpler filtration requirements.

5-3 General Performance Characteristics

In the following subsections, torque-speed characteristics, ripple factor of the armature current and the input power factor of system under consideration are investigated. These characteristics are calculated at a chopping frequency of *1200 Hz*. The modulation index γ is considered as the control parameter.

(A) Torque-Speed Characteristics

The torque-speed characteristics are shown in figure (8). The boundary limit between the continuous and the discontinuous conduction regions (critical operating conditions) is shown by the dotted curve. For a given modulation index, speed regulation is quite good over most of the operating range, where the armature current is continuous. However, under light loading, speed regulation becomes poor, owing to the nature of the load current, which becomes discontinuous. However, the figure shows that the system mainly operates in the continuous mode of operation, even at no-load condition. The chance for the system to operate in this mode increases if the modulating frequency and/or the armature time-constant are made higher, as previously explained.

(B) Ripple Factor of the Armature Current

The ripple of the armature current is an essential parameter that should be less than a certain permissible value, usually specified by the manufacturer. Figure (9) shows the variations of the ripple factor *RF* over the complete range of operation. The figure shows that for a given modulation index, the ripple factor increases with speed. The tendency of the curve to change its trend for a given modulating index, is due to the change of the mode of operation, from the continuous mode to the discontinuous mode.

(C) Input Power Factor

Figure (10) shows the variations of the input power factor *PF* versus the motor speed. The power factor has almost fixed amplitude proportional to the modulation index. The tendency of the power factor to change its level occurs when the load current becomes discontinuous.

6 CONCLUSIONS

Steady-state modelling of a uniform pulse width modulated three-phase AC-to-DC converter-fed DC motor drive is accomplished. The developed model is presented in a generalized mathematical form that is applicable irrespective of the chopping frequency. The model and its solution procedure are experimentally verified using a testing model implemented for this purpose. The effects of the armature time-constant and the chopping frequency on the nature of the armature current are investigated. The results show that higher armature time-constant and higher chopping frequency (up to a certain level) improve the chances for the system to operate in the continuous mode, and hence are expected to provide better performance characteristics. The main general performance characteristics of the system are also

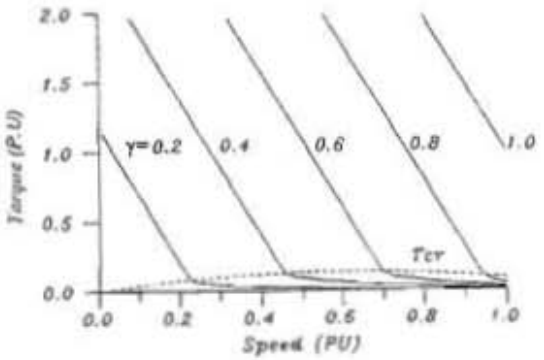

Figure (8): Torque-speed characteristics.

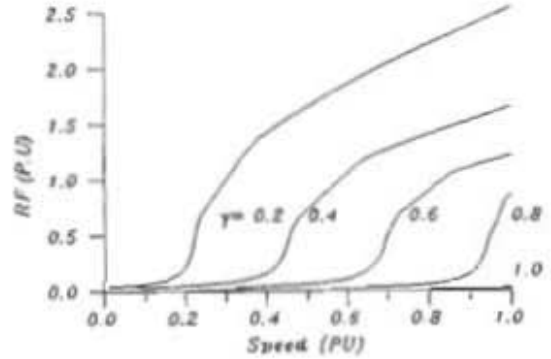

Figure (9): Ripple factor of the armature current versus speed.

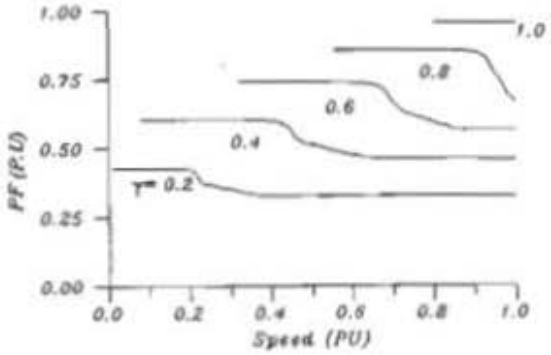

Figure (10): Input power factor versus speed.

investigated over the complete range of operation with γ being the parameter. The paper will be followed by a detailed study of the performance characteristics of the system under specific torque-speed load characteristics (i.e., fan-type and constant-torque load characteristics).

7 REFERENCES

[1] T. Kataoka K. Mizumachi, and Miyairi, "A Pulsewidth Controlled AC to DC Converter to Improve Power Factor and Waveform of AC Line Current", IEEE Trans. Ind. Appl., Vol.IA-15, No.6, pp.670-675, Nov./Dec. 1979.

[2] S. Doradla, C. Nagamani, and S. Sanyal, "A Sinusoidal Pulse-width Modulated Three-Phase AC to DC Converter-Fed DC Motor Drive", IEEE Trans. Ind. Appl., Vol.IA-21, No.6, pp.1394-1408, Nov./Dec. 1985.

[3] S. Biswas, M. Mahesh, and B. Iyenger, "Simple New PWM Patterns for Thyristor Three-Phase AC to DC Converters", Proc. Inst. Elec. Eng., Pt.B, Vol.133, No.6, pp.354-358, Nov. 1986.

[4] S. Biswas, B. Basak, and M. Swamy, "A Three-Phase Half-Controlled Rectifier with Pulse Width Modulation", IEEE Trans. on Inds. Elect., Vol.38, No.2, pp.121-125, April 1991.

[5] S. A. Hamed, "Steady-State Modelling of a Uniform Pulse-Width Modulated Single-phase AC-to-DC Converter-Fed DC Motor Drive", ETEP Vol.3, No.5, pp. 379-368. Sep./Oct. 1993.

[6] S. A. Hamed, and M. Shaderma, "Modelling and implementation of a Sinusoidal-Pulse-Width-Modulated DC Drive System", INT. J. Electronics, Vol.75, No.6, pp. 1295-1310, 1993.

[7] S. A. Hamed, and B. J. Chalmers, "Performance Evaluation of Variable-Speed DC Drive With Sinusoidal PWM Control", Sixth International Conference on "Electrical Machines and Drive", pp. 61-66, Oxford U.K., September 1993.

8 APPENDIX

The motor used for the verification of the developed model is a separately-excited DC motor having the following parameters:

- Rated output power: *1250 W*
- Rated terminal voltage: *220 V*
- Rated armature current: *7.5 A*.
- Rated speed: *2300 RPM*.
- Measured armature resistance: *6 Ω*
- Measured armature inductance: *20 mH*.
- Design-excitation constant *K*: *0.727 V.Sec. rad*.

NOMENCLATURE

f_s Supply frequency (*Hz*).
f_o Output frequency (*Hz*).
f_c Chopping frequency (*Hz*).
M Chopping-to-supply frequency ratio = f_c/f_s.
N Number of pulses per output period of symmetry (i.e., $\pi/3$).
γ Modulation index.
T Chopping period.
ω Electrical angular velocity = $2\pi f_s$ (*rad/sec*).
x A parameter = ωt (*rad*).
R Armature effective resistance (Ω).
L Armature effective inductance (*H*).
τ Armature inductance-to-resistance ratio = L/R (sec.).
τ_o Original armature-to-inductance ratio.
X Armature reactance at supply frequency = ωL (Ω).
Z Armature impedance at supply frequency = $(R^2+X^2)^{1/2}$ (Ω).
ϕ Load phase angle at supply frequency = $\tan^{-1}(X/R)$.
ρ A constant = $-L/\tan(\phi)$.
Vp Maximum amplitude of the line voltage (*V*).
Ip Peak current = Vp/Z (*A*).
V_r Terminal rated voltage of the motor (*V*).
N Speed in (*RPM*).
K Design-excitation constant of the motor (*V.sec./rad*).
I_a Average value of the armature current (*A*).
V_a Average value of the armature voltage (*V*).
T_a Average value of the developed torque = $K.I_a$ (*N.m*).
ω_m mechanical angular velocity = $2\pi N/60$ (*rad./sec.*)
E Back EMF = $K\omega_m = V_a - R.I_a$ (*V*).